

# 1 Linking the complementary evaporation relationship with the Budyko 2 framework for ungauged areas in Australia

3 Daeha Kim<sup>1</sup>, Minha Choi<sup>2</sup>, Jong Ahn Chun<sup>3</sup>

4 <sup>1</sup>Department of Civil Engineering, Jeonbuk National University, Jeonju, Jeollabuk-do, 54896, South Korea

5 <sup>2</sup>Department of Water Resources, Sungkyunkwan University, Suwon, Gyeonggi-do, 16419, South Korea

6 <sup>3</sup>Prediction Research Department, APEC Climate Center, Busan, 48058, South Korea

7  
8 *Correspondence to:* Jong Ahn Chun (jachun@apcc21.org)

9 **Abstract.** While the calibration-free complementary relationship (CR) has performed excellently in predicting terrestrial  
10 evapotranspiration ( $ET_a$ ), how to determine the Priestley-Taylor coefficient ( $\alpha_c$ ) is still questionable. In this work, we evaluated  
11 this highly utilizable method, which only requires atmospheric data, with in-situ flux observations and basin-scale water  
12 balance estimates ( $ET_{wb}$ ) in Australia, proposing how to constrain it with a traditional Budyko equation for ungauged locations.  
13 We found that the CR method with a constant  $\alpha_c$  transferred from fractional wet areas performed poorly in reproducing the  
14 mean annual  $ET_{wb}$  in unregulated river basins, and it underperformed sophisticated physical, machine-learning, and land  
15 surface models in closing grid-scale water balance. This problem was remedied by linking the CR method with a traditional  
16 Budyko equation that allowed an upscaling of the optimal  $\alpha_c$  from gauged basins to ungauged locations. The proposed CR-  
17 Budyko framework enabled us to reflect climate conditions in  $\alpha_c$ , leading to more plausible  $ET_a$  estimates in ungauged areas.  
18 The spatially varying  $\alpha_c$  conditioned by local climates made the CR method outperformed the three  $ET_a$  models in reproducing  
19 the grid-scale  $ET_{wb}$  across the Australian continent. We here argued that the polynomial CR with a constant  $\alpha_c$  could result in  
20 biased  $ET_a$ , and it can be constrained by local climate conditions for improvement.

## 21 1 Introduction

22 Evapotranspiration ( $ET_a$ ) plays a pivotal role in water and energy exchanges between the land and the atmosphere.  
23 On the global scale, more than 60% of terrestrial precipitation (P) returns to the atmosphere through plants' vascular systems  
24 and soil pores, while consuming over 70% of surface net radiation (Trenberth et al., 2007; 2009). Since it is tightly coupled  
25 with carbon cycles, abnormally low  $ET_a$  would indicate food insecurity and low ecosystem sustainability (Jasechko, 2018;  
26 Kyatengerwa et al., 2020; Pareek et al., 2020; Swann et al., 2016). In severe cases,  $ET_a$  limited by deficient soil moisture can  
27 lead to extreme heatwaves that further propagate the water deficit in space and time (Miralles et al., 2014; Mueller and  
28 Seneviratne, 2012; Schumacher et al., 2022).

29           Despite great community efforts for sharing in-situ observations (e.g., Baldocchi, 2020; Novick et al., 2018), ET<sub>a</sub>  
30 gauging networks are unevenly established over land surfaces and often subjected to error sources (e.g., unclosed energy  
31 balance) and limited data lengths (Ma et al., 2021). Inevitably, modeling approaches are needed to predict ET<sub>a</sub> in ungauged or  
32 poorly gauged areas, or to characterize it on a long timescale in a large area. Hence, various approaches have been proposed  
33 including physical models (e.g., Martens et al., 2017; Zhang et al., 2016), machine-learning techniques (e.g., Jung et al., 2019;  
34 Tramontana et al., 2016), and conceptual land surface schemes (e.g., Guimberteau et al., 2018; Haverd et al., 2018).

35           Those modeling approaches typically require P data and land surface information (e.g., remote-sensing vegetation  
36 indices) to quantify available soil moisture to the vaporization process. However, due in part to uncertainty associated with P  
37 data (Sun et al., 2018) and model structures (Samaniego et al., 2017; Zhang et al., 2019), resulting ET<sub>a</sub> estimates have shown  
38 substantial disparities. In the comprehensive intercomparison by Pan et al. (2020), for example, the 14 advanced land surface  
39 models generated the global mean ET<sub>a</sub> varying widely between 450 mm a<sup>-1</sup> and 700 mm a<sup>-1</sup>. Such a large incongruity in  
40 modeled ET<sub>a</sub> was also found by the earlier Global Soil Wetness Project (Schlosser and Gao, 2010), suggesting that an  
41 alternative method is necessary to circumvent the uncertainty sources.

42           A practical method to simulate ET<sub>a</sub> without P data and land-surface schemes is the complementary relationship (CR)  
43 of evaporation (Bouchet, 1963). It uses the evident fact that the air over a water-limited surface amplifies its vapor pressure  
44 deficit (VPD), while this effect disappears when the same surface is amply wet (Chen and Buchberger, 2018; Ramírez et al.,  
45 2005; Zhou et al., 2019). Based on the atmospheric self-adjustment, numerous equations have been formulated to predict ET<sub>a</sub>  
46 only using routine meteorological data (e.g., Anayah and Kaluarachchi, 2014; Crago and Crowley, 2005; Crago and Qualls,  
47 2013; Hobbins et al., 2004; Huntington et al., 2011; Kahler and Brutsaert, 2006 among others). In particular, the definitive  
48 derivation by Brutsaert (2015) and the following modifications (Crago et al., 2016; Crago and Qualls, 2021; Szilagyi, 2021;  
49 Szilagyi et al., 2017) provided strong physical foundations to Bouchet's (1963) early principle. They have excellently predicted  
50 ET<sub>a</sub> at various spatial and temporal scales (e.g., Brutsaert et al., 2017, 2020; Crago and Qualls, 2018; Ma et al., 2019, 2021;  
51 Ma and Szilagyi, 2019), and allowed users to assess vegetation droughts over national and continental areas (e.g., Kim et al.,  
52 2019, 2021; Kyatengerwa et al., 2020).

53           Nevertheless, the definitive CRs still require at least some ET<sub>a</sub> data to calibrate the parameters that determine the  
54 hypothetical wet-surface evaporation (ET<sub>w</sub>; Qualls and Crago, 2020); thus, they are not fully free of P data or parameterization.  
55 For instance, Brutsaert et al. (2020) calibrated the single parameter of Brutsaert's (2015) CR with flux observations and basin-  
56 scale P and runoff (Q) data to estimate annual ET<sub>a</sub> across the globe. For evaluating four definitive CRs from Brutsaert's (2015)  
57 derivation, Crago et al. (2022) also calibrated their parameters by eddy-covariance flux observations. To date, Szilagyi et al.  
58 (2017) has proposed the only CR formulation that purely uses routine meteorological data; however, it depends on a  
59 questionable assumption that the parameter for ET<sub>w</sub> is constant over a large continental area, being counterfactual to  
60 experimental studies on the Priestley and Taylor (1972) coefficient (e.g., Assouline et al., 2016; Baldocchi et al., 2016; Parlange  
61 and Katul, 1992; Wang et al., 2014). Given the complex space-time links between climate, soil, and vegetation (Hagedorn et

62 al., 2019; Mekonnen et al., 2019; Rodriguez-Iturbe, 2000), the aerodynamic component of  $ET_w$  is unlikely represented by a  
63 fixed fraction of the net radiation.

64 Owing to the data required for parameter calibration, the state-of-the-art CR formulations might not be applicable in  
65 ungauged locations. In part, this problem can be mended by an additional constraint for determining the essential parameters,  
66 and the traditional Budyko framework can come into play. A Budyko function (e.g., Fu, 1981; Yang et al., 2008) explains the  
67 mean ratio of  $ET_a$  to  $P$  (i.e., surface water balance) simply by climatological aridity and a few implicit parameters,  
68 simultaneously closing the surface energy budget (Mianabadi et al., 2020). Although Bouchet's principle has often been linked  
69 with the water balance describe by Budyko functions (e.g., Carmona et al., 2016; Chen and Buchberger, 2018; Lhomme and  
70 Moussa, 2016; Zhang and Burtsaert, 2021), this theoretical link has been ignored when predicting  $ET_a$  by the definitive CRs.  
71 Kim and Chun (2021) explicitly showed that the atmospheric self-adjustment is tightly coupled with the climatological aridity  
72 within a Budyko function. This implicates that the optimal parameter for a definitive CR should vary with climates rather than  
73 staying constant.

74 In this work, we showed that a Budyko equation could become an important physical constraint when predicting  $ET_a$   
75 by a definitive CR over a continental area. Here, a practical approach was proposed to determine the parameters reasonably in  
76 ungauged locations via a case study for the Australian continent, where the performance of the CR method remained unknown  
77 in many parts. Based on the analytical relationship between the CR and the Budyko framework, we showed why the parameter  
78 of the CR is not independent of local climate conditions, and addressed how to reflect spatially varying climates in its essential  
79 parameter.

## 80 **2 Methodology and data**

### 81 **2.1 The polynomial CR by Szilagyi et al. (2017)**

82 For the case study, we employed the calibration-free CR formulated by Szilagyi et al. (2017). It describes the  
83 atmospheric self-adjustment to surface moisture conditions using three evaporation rates, namely,  $ET_a$ ,  $ET_w$ , and the potential  
84 evaporation ( $ET_p$ ).  $ET_a$  is the actual moisture flux from a land surface to the atmosphere, and  $ET_w$  is the hypothetical  $ET_a$  rate  
85 that should occur with ample water availability.  $ET_p$  is the atmospheric capacity to receive water vapor that responds actively  
86 to soil moisture conditions. By defining the two dimensionless variables,  $x \equiv ET_w/ET_p$  and  $y \equiv ET_a/ET_p$ , Szilagyi et al. (2017)  
87 derived a polynomial function from four definitive boundary conditions.

88 Under ample water conditions,  $ET_p$  does not deviate from  $ET_w$  and  $ET_a$  (i.e.,  $ET_p = ET_w = ET_a$ ); hence, the  
89 corresponding zero-order boundary condition is (i)  $y = 1$  for  $x = 1$ . In contrast,  $ET_a$  must be nil over a desiccated surface (i.e.,  
90  $y = 0$ ), and by energy balance, the surface net radiation should be fully transformed to the sensible heat flux. Then, the  
91 atmospheric VPD would be amplified at the maximum level with the same net radiation and wind speed. Defining the  
92 maximum  $ET_p$  rate as  $E_{pmax}$ , another zero-order boundary condition is given as (ii)  $y = 0$  for  $x = x_{min} \equiv ET_w/E_{pmax}$ . When  $x = 1$   
93 (i.e., ample water), changes in  $ET_a$  would be controlled by changes in  $ET_w$ , yielding a first-order boundary condition as: (iii)

94  $dy/dx = 1$  for  $x = 1$ . Over a desiccated surface,  $ET_a$  stays at zero even when  $ET_w$  or  $ET_p$  changes; thus, another first-order  
 95 boundary condition becomes (iv)  $dy/dx = 0$  for  $x = 0$ . The simplest polynomial equation satisfying the four boundary conditions  
 96 is:

$$97 \quad y = 2X^2 - X^3, \quad (1a)$$

98 where,  $X$  rescales the variable  $x$  into  $[0, 1]$  as:

$$99 \quad X = \frac{x-x_{\min}}{1-x_{\min}} = \frac{E_{p\max}-ET_p-ET_w}{E_{p\max}-ET_w-ET_p}. \quad (1b)$$

00 Eq. (1) allows users to estimate  $ET_a$  with no land-surface information, because  $ET_p$ ,  $ET_w$ , and  $E_{p\max}$  are all obtainable  
 01 from a set of net radiation, air temperature, dew-point temperature, and wind speed data.  $ET_p$  and  $E_{p\max}$  can be estimated by  
 02 the Penman (1948) equation:

$$03 \quad ET_p = \frac{\Delta(T_a) R_n}{\Delta(T_a)+\gamma \lambda_v} + \frac{\gamma}{\Delta(T_a)+\gamma} f_u VPD, \quad (2)$$

$$04 \quad E_{p\max} = \frac{\Delta(T_{dry}) R_n}{\Delta(T_{dry})+\gamma \lambda_v} + \frac{\gamma}{\Delta(T_{dry})+\gamma} f_u e_s(T_{dry}), \quad (3)$$

05 where,  $\Delta(\cdot)$  is the slope of the saturation vapor pressure curve ( $\text{kPa } ^\circ\text{C}^{-1}$ ),  $T_a$  is the mean air temperature ( $^\circ\text{C}$ ),  $\gamma$  is the  
 06 psychrometric constant ( $\text{kPa } ^\circ\text{C}^{-1}$ ),  $R_n$  is the surface net radiation less the soil heat flux ( $\text{MJ m}^{-2} \text{ d}^{-1}$ ),  $\lambda_v$  is the latent heat of  
 07 vaporization ( $\text{MJ kg}^{-1}$ ),  $f_u = 2.6 (1 + 0.54 u_2)$  is the Rome wind function ( $\text{mm d}^{-1} \text{ kPa}^{-1}$ ), where  $u_2$  is the 2-m wind speed ( $\text{m s}^{-1}$ ),  
 08 and  $VPD$  is calculated by  $e_s(T_a)$  minus  $e_s(T_{dew})$ , where  $e_s(\cdot)$  is the saturation vapor pressure ( $\text{kPa}$ ) and  $T_{dew}$  is the dew point  
 09 temperature ( $^\circ\text{C}$ ).

10  $T_{dry}$  in Eq. (3) is the air temperature ( $^\circ\text{C}$ ) at which the lower atmosphere is devoid of humidity presumably by the  
 11 adiabatic drying process:

$$12 \quad T_{dry} = T_{wb} + \frac{e_s(T_{wb})}{\gamma} = T_a + \frac{e_s(T_{dew})}{\gamma}, \quad (4)$$

13 where,  $T_{wb}$  is the wet-bulb temperature ( $^\circ\text{C}$ ) at which the saturation vapor pressure curve intersects with the adiabatic wetting  
 14 line. Thus, it is obtained by:

$$15 \quad \gamma \frac{T_{wb}-T_{avg}}{e_s(T_{wb})-e_a} = -1. \quad (5)$$

16 To estimate  $ET_w$  in Eq. (1b), the Priestly-Taylor (1972) equation has been a typical choice (e.g., Brutsaert, 2015;  
 17 Crago et al., 2016; Han and Tian, 2018; Szilagyi et al., 2017):

$$18 \quad ET_w = \alpha_e \frac{\Delta(T_w) R_n}{\Delta(T_w)+\gamma \lambda_v}, \quad (6)$$

19 where,  $\alpha_e$  is the Priestley-Taylor coefficient ranging usually within  $[1.10, 1.32]$  (Szilagyi et al., 2017), and  $T_w$  is the wet-  
 20 environment air temperature ( $^\circ\text{C}$ ).  $T_w$  can be approximated with the wet-surface temperature ( $T_{ws}$ ), because the vertical air  
 21 temperature gradient is negligible under a wet environment. Given its independence on areal extent (Szilagyi and Schepers,  
 22 2014),  $T_{ws}$  can be approximated by the implicit Bowen ratio ( $\beta$ ) of a small wet patch:

$$23 \quad \beta = \frac{R_n-ET_p}{ET_p} \approx \gamma \frac{T_{ws}-T_a}{e_s(T_{ws})-e_s(T_{dew})}. \quad (7)$$

24 Eq. (7) assumes that the available radiation for the wet patch is close to that of the drying surface (Szilagyi et al., 2017).  $T_{ws}$   
 25 might be higher than  $T_a$  when the air is close to saturation. In such a case,  $T_{ws}$  should be capped by  $T_a$  when calculating  $ET_w$ .

26 The single parameter of the polynomial CR, i.e.,  $\alpha_e$ , is analytically obtainable by inserting the Priestley-Taylor  
 27 equation into the Bowen ratio of a wet environment (Szilagyi et al., 2017):

$$28 \quad \alpha_e = \frac{[\Delta(T_a) + \gamma][e_s(T_{ws}) - e_s(T_{dew})]}{\Delta(T_a)[\{e_s(T_{ws}) - e_s(T_{dew})\} + \gamma(T_{ws} - T_a)]}, \quad (8)$$

29 where,  $\alpha_e$  must be fall within the theoretical limit of  $[1, 1 + \gamma/\Delta(T_a)]$  (Priestley and Taylor, 1972).

## 30 2.2 The analytical relationship between the polynomial CR and a Budyko function

31 Since Eq. (8) is applicable only in a wet environment, Szilagyi et al. (2017) identified wet locations in a continental  
 32 area based on the fact that the air close to saturation should have high relative humidity (RH) with  $T_{ws} > T_a$ . Thus, they  
 33 calculated  $\alpha_e$  values at locations with  $RH > 90\%$  and  $T_{ws} > T_a + 2$  °C, and the average value was used to predict  $ET_a$  for a  
 34 continental area. However, the spatially constant  $\alpha_e$  is unlikely suitable in such a large area under diverse climates, because  
 35 the equilibrium between the atmosphere and the underlying surface is intertwined with the partitioning of P to  $ET_a$  and Q over  
 36 the surface.

37 Kim and Chun (2021) analytically related Eq. (1) with the traditional Turc-Mezentsev equation, and found that the  
 38 self-adjustment of  $ET_p$  (i.e.,  $x$ ) is tightly linked with climatological aridity and land properties. For the independence between  
 39 P and ‘the possible maximum  $ET_a$ ’ of the Budyko framework, Kim and Chun (2021) reformulated the traditional equation with  
 40  $\Phi_0 \equiv ET_w/P$  instead of the commonly used aridity index ( $\Phi \equiv ET_p/P$ ) as:

$$41 \quad \frac{ET_a}{P} = \frac{ET_w}{P} \left[ \frac{1}{1 + \left(\frac{ET_w}{P}\right)^n} \right]^{\frac{1}{n}} = \frac{xET_p}{P} \left[ \frac{1}{1 + \left(\frac{xET_p}{P}\right)^n} \right]^{\frac{1}{n}}, \quad (9)$$

42 where, the parameter  $n$  implicitly represents the factors affecting the P partitioning other than the climatic drivers. By dividing  
 43 Eq. (9) by  $\Phi$ , it is found that the Budyko equation (9) is intertwined with the Eq. (1a):

$$44 \quad y = \frac{ET_a}{ET_p} = 2X^2 - X^3 = \left[ \frac{x^n}{1 + x^n \Phi^n} \right]^{\frac{1}{n}}. \quad (10)$$

45 Eq. (10) implies that the self-adjustment of  $ET_p$  (i.e.  $x$ ) is tightly related with the climatic condition (i.e.,  $\Phi$ ), and the land  
 46 property (i.e.,  $n$ ).

47 While the  $x$  and  $n$  can be achievable from a set of  $ET_a$ ,  $ET_p$ ,  $E_{pmax}$ , and P values by inverting Eq. (10), such an approach  
 48 is not applicable in locations with no  $ET_a$  data. To quantify  $x$  values only using  $ET_p$ ,  $E_{pmax}$ , and P, Kim and Chun (2021)  
 49 developed a regression equation between  $x$  and  $\Phi$ ,  $x_{min}$ , and  $n$  values from the 513 gauged river basins over the world. We used  
 50 the same regression-based regionalization. Considering  $x_{min} = xET_p/E_{pmax}$ , the non-linear Eq. (10) can be approximated by a  
 51 multiple regression as:

$$52 \quad \tilde{x} = b_0 + b_1 \ln(\Phi) + b_2 \ln(ET_p/E_{pmax}) + b_2 \ln(n), \quad (11)$$

53 where,  $\tilde{x}$  is the approximate ratio of  $ET_w$  to  $ET_p$ , and  $b_0$ ,  $b_1$ , and  $b_2$  are the intercept and the regression coefficients, respectively.  
 54 Since the implicit parameter  $n$  is unavailable in ungauged locations, Eq. (11) needs to be further simplified by neglecting the  
 55 last term:

$$56 \quad \tilde{x} \approx c_0 + c_1 \ln(\Phi) + c_2 \ln(ET_p/E_{pmax}), \quad (12)$$

57 where,  $c_0$ ,  $c_1$ , and  $c_2$  are the intercept and the coefficients of the approximated regression.

58 If  $\tilde{x}$  is known by the regression Eq. (12), the parameter  $\alpha_e$  can be estimated using the Priestley-Taylor equation as:

$$59 \quad \tilde{\alpha}_e = \tilde{x} \frac{ET_p}{ET_{eq}} \quad (13a)$$

$$60 \quad ET_{eq} = \frac{\Delta(T_w) R_n}{\Delta(T_w) + \gamma \lambda_v} \quad (13b)$$

61 where,  $\tilde{\alpha}_e$  is the Priestley-Taylor coefficient that approximately satisfies the CR and the Budyko equations together, and  $ET_{eq}$   
 62 is the equilibrium evapotranspiration ( $\text{mm d}^{-1}$ ) at which VPD is nil under a wet environment. It should be noted that  $P$ ,  $ET_p$ ,  
 63  $E_{pmax}$ , and  $ET_{eq}$  within Eqs. (9)-(13) must be on a timescale where the Turc-Mezentsev equation is valid (typically longer than  
 64 a year), and  $\tilde{\alpha}_e$  is still bounded by  $[1, 1 + \gamma/\Delta(T_a)]$ .

### 65 **2.3 Atmospheric forcing, eddy-covariance, and runoff data**

66 We examined the CR-Budyko combined framework in the Australian continent lying within  $[10^\circ\text{--}45^\circ\text{S}, 113^\circ\text{--}155^\circ\text{E}]$ .  
 67 The required atmospheric forcing data ( $R_n$ ,  $T_a$ ,  $T_{dew}$ , and  $u_2$ ) were collected from the advanced ERA5-Land reanalysis archive  
 68 (Muñoz-Sabater et al., 2021) of the European Centre for Medium-Range Weather Forecasts (<https://cds.climate.copernicus.eu>;  
 69 last access on Dec-10/2021). The monthly averages of surface latent and sensible heat fluxes, 2-m air temperature, 2-m dew-  
 70 point temperature, and 10-m U and V wind speed components at  $0.1^\circ \times 0.1^\circ$  were downloaded for 1981–2020.  $R_n$  was calculated  
 71 by summing the two heat fluxes, and the 10-m wind speed components were converted to  $u_2$  using the logarithmic wind profile  
 72 (Allen et al., 1998).

73 We also collected the Australian edition of the Catchment Attributes and Meteorology for Large sample Studies  
 74 (CAMELS; Fowler et al., 2021) series of datasets (available at <https://doi.org/10.1594/PANGAEA.921850>; last access on Sep-  
 75 27/2021). The CAMELS datasets comprise daily time series of 19 hydrometeorological variables at 222 unregulated river  
 76 basins in Australia up to 2014, and we selected the 71 basins larger than  $500 \text{ km}^2$  to contain at least five CR  $ET_a$  estimates  
 77 within the boundaries. The water-balance  $ET_a$  ( $ET_{wb}$ ) (i.e.,  $ET_{wb} \approx \Sigma P - \Sigma Q$ ) of each basin was calculated for the two periods of  
 78 1981–1997 and 1998–2014. The mean annual  $ET_{wb}$  for the former period was used for the regressions with Eqs. (11) and (12),  
 79 and the predicted  $ET_a$  was evaluated against the latter.

80 As a point-scale evaluation dataset, the annual flux observations were taken from the 15 eddy-covariance stations  
 81 (Table 1) of the FLUXNET2015 archive (<https://fluxnet.org/>; last access on Jul-1/2021). We chose the flux towers with 2 or  
 82 more annual means, and adopted the energy-balance-corrected latent heat flux observations with the quality measures

83 'LE\_F\_MDS\_QC' higher than 0.70. Given the fine resolution of the ERA5-Land forcing data, we believed that the  $ET_a$   
84 estimates by CR could be directly compared with the point-scale observations.

85 In addition, as a grid-scale evaluation reference, the SILO P data at  $0.01^\circ \times 0.01^\circ$  were collected from the Queensland  
86 government (<https://www.longpaddock.qld.gov.au/silo/gridded-data>; last access on Jun-01/2021) together with the Global  
87 RUNoff (GRUN) ENSEMBLE (Ghiggi et al., 2021) (<https://doi.org/10.6084/m9.figshare.12794075>; last access on Oct-  
88 1/2021). The global Q data were produced at  $0.5^\circ \times 0.5^\circ$  using a machine-learning algorithm trained by in-situ streamflow  
89 observations, and potential errors were reduced by simulations with 21 sets of atmospheric forcing (Ghiggi et al., 2021). The  
90 SILO P was used to calculate  $\Phi = P/ET_p$  at each grid of the forcing data. After bilinearly unifying the resolutions of SILO P  
91 and GRUN Q data, we also calculated the mean annual  $ET_{wb}$  for 1998–2014 at  $0.5^\circ \times 0.5^\circ$  over the entire Australian continent.

92 Against the grid-scale  $ET_{wb}$  estimates, performance of the polynomial CR was also compared with three  $ET_a$  products  
93 from a physical, a machine-learning, and a land-surface model. The physical model was the Global Land Evaporation  
94 Amsterdam Model (GLEAM) v3.2 (Martens et al., 2017; <https://www.gleam.eu>; last access on Jun-03/2020) based on the  
95 Priestley-Taylor equation constrained by microwave-derived soil moisture, surface temperature, and vegetation optical depth.  
96 The machine-learning  $ET_a$  product was the FluxCom (<http://www.fluxcom.org/>; last access Mar-18/2019) that upscaled in-situ  
97 observations at 224 eddy-covariance towers using 11 algorithms (Jung et al., 2019). We used the version forced by the  
98 CRUNCEPv8 that has the longest data length from 1950 to 2016. The land-surface-model product was the ERA5-Land  
99 monthly  $ET_a$  (<https://cds.climate.copernicus.eu>; last access on Jul-7/2021) simulated by the advanced Hydrology Tiled  
00 ECMWF Scheme for Surface Exchanges over Land scheme (Balsamo et al., 2015). All the modeled  $ET_a$  datasets were  
01 bilinearly regridded to  $0.5^\circ \times 0.5^\circ$  for 1998–2014 to be compared with the grid-scale  $ET_{wb}$  data.

## 02 **3 Results**

### 03 **3.1 Performance of the calibration-free CR in Australia**

04 Figure 1a depicts the spatial distribution of the inverted aridity index ( $\Phi^{-1} = P/ET_p$ ) that can traditionally categorize  
05 climate conditions. The mean ratios between SILO P and  $ET_p$  for 1998–2014 indicated that 83% of the Australian land surfaces  
06 were under arid ( $\Phi^{-1} < 0.2$ ) and semi-arid climates ( $0.2 < \Phi^{-1} < 0.5$ ). Semi-humid ( $0.5 < \Phi^{-1} < 0.65$ ) and humid climates ( $\Phi^{-1} >$   
07  $0.65$ ) were only found in the northern and southeastern coastal areas and the southwestern edge where major cities and  
08 agricultural lands have developed. Despite the high aridity, hyper-arid climates ( $\Phi^{-1} < 0.05$ ) were not found in Australia.

09 We first examined the calibration-free approach by Szilagyi et al. (2017) that only uses the meteorological forcing  
10 inputs. The blue-colored points in Figure 1a are the locations with  $RH > 90\%$  and  $T_{ws} > T_a + 2^\circ C$ , at which the  $\alpha_e$  values from  
11 Eq. (8) were within  $1.15 \pm 0.047$  (mean  $\pm$  standard deviation). Though the two conditions were met in some mountainous areas  
12 in the southeastern part, we excluded them because unexpectedly high  $\alpha_e$  values were obtained. The mean  $\alpha_e = 1.15$  fell within

13 the theoretical limits, and was equal to the value used in the prior studies in China (Ma et al., 2019) and the conterminous U.S.  
14 (Ma and Szilagyi, 2019).

15 Using the CR with  $\alpha_e = 1.15$ , we predicted  $ET_a$  over the entire Australian continent (Figure 1b). The distribution of  
16 the resulting mean  $ET_a$  for 1998–2014 was coherent with that of  $\Phi^{-1}$ . The mean CR  $ET_a$  ranged in  $262 \pm 85.3 \text{ mm a}^{-1}$  and  $547$   
17  $\pm 173 \text{ mm a}^{-1}$  under arid and semi-arid climates, respectively. On the other hand, CR  $ET_a$  in semi-humid and humid locations  
18 were much higher in  $886 \pm 187 \text{ mm a}^{-1}$  and  $1,010 \pm 213 \text{ mm a}^{-1}$ , respectively. The calibration-free CR predicted the continental  
19 mean  $ET_a$  as high as  $489 \text{ mm a}^{-1}$  for 1981–2012, and it was about 11.3% higher than the estimate for the same period ( $439 \text{ mm}$   
20  $\text{a}^{-1}$ ) by Zhang et al. (2016). The mean fraction of  $ET_a$  to P for 1998–2014 (97%) was larger than the typical  $ET_a$  value in  
21 Australia (~90%; Glenn et al., 2011), implicating that the constant  $\alpha_e = 1.15$  seemed to make the CR overrate  $ET_a$ .

22 The overestimation of the calibration-free CR was confirmed by the flux observations and the basin-scale  $ET_{wb}$   
23 (Figure 2). The percent bias (p-bias) of CR  $ET_a$  to the point-scale annual  $ET_a$  was +10.4%, while it became more than doubled  
24 when compared to the basin-scale  $ET_{wb}$ . Though the Pearson correlation coefficients (Pearson r) were significantly high  
25 between the CR  $ET_a$  and the two evaluation references, the low Nash-Sutcliffe efficiency (NSE) to  $ET_{wb}$  implicates that the  
26 CR method could perform poorly in wet river basins. The regression slopes in Figure 2 also indicate that the calibration-free  
27 CR tends to increasingly overestimate as climate becomes wetter. The root mean square error (RMSE) of CR  $ET_a$  to  $ET_{wb}$  was  
28 higher than to the point observations. Although it appeared to perform acceptably at the 15 flux towers, the CR method  
29 produced considerable biases in the 71 CAMELS basins. The performance measures were not as excellent as the same CR  
30 method had shown in the U.S. (Ma et al., 2021, Ma and Szilagyi, 2019; Kim et al., 2019) and in China (Ma et al., 2019).

31 One may argue that the mean  $\alpha_e$  derived from fractional wet areas is unlikely representative of the large Australian  
32 continent, and this might introduce the biases to CR  $ET_a$  estimates. Hence, we re-simulated CR  $ET_a$  with Ma et al.'s (2021)  
33 estimate ( $\alpha_e = 1.10$ ) from a global-scale analysis. Figure 3a shows that the predicted  $ET_a$  became nearly unbiased at the 15 flux  
34 tower locations, and seemingly suggests that the decreased  $\alpha_e$  could become a solution to improving the CR method.  
35 Nevertheless, the fixed  $\alpha_e$  still made the CR overestimate  $ET_a$  in the CAMELS basins under (semi-)humid climates, albeit  
36 slightly ameliorated (Figure 3b).

### 37 **3.2 The empirical relationship between $\tilde{x}$ to climate conditions**

38 Figures 2 and 3 imply that the calibration-free CR with a fixed  $\alpha_e$  was unlikely good at closing local water balance  
39 particularly in (semi-)humid river basins. To resolve this problem with the CR-Budyko framework, first we estimated the  
40 climatological  $x$  and the parameter  $n$  of the CAMLES basins using Eq. (10) with the mean annual  $ET_{wb}$ , P,  $ET_p$ , and  $E_{pmax}$  for  
41 1981-1997. Figure 4a-c illustrates the scatter plots between the resultant  $x$  and corresponding  $\Phi$ ,  $ET_p/E_{pmax}$ , and  $n$  values.  
42 Pearson r values between the  $x$  and the other three variables were -0.88, -0.59, and 0.44, respectively (significant at 1% level),  
43 suggesting that the self-adjustment of  $ET_p$  is not only correlated with climate conditions, but with land surface properties at

44 least in part. By regressing between the  $x$  values and the log-transformed  $\Phi$ ,  $ET_p/E_{pmax}$  and  $n$ , we obtained an empirical  
45 relationship that enables to spatially predict the mean annual ratio of  $ET_w$  to  $ET_p$  as:

$$46 \quad \tilde{x} = 0.949 - 0.204 \ln(\Phi) + 0.231 \ln(ET_p/E_{pmax}) + 0.0712 \ln(n). \quad (14)$$

47 The regression coefficients were all significant at 1% level, and the coefficient of determination ( $R^2$ ) was 0.98. The regression  
48 equation was further approximated by discarding  $n$  from the explanatory variables:

$$49 \quad \tilde{x} = 1.023 - 0.220 \ln(\Phi) + 0.210 \ln(ET_p/E_{pmax}). \quad (15)$$

50 The  $R^2$  value of Eq. (15) declined to 0.93. We found that the simple regression between  $x$  and  $\Phi$  further reduced  $R^2$  to 0.90.  
51 While the heterogeneous land properties exert non-negligible influences, the regression analyses imply that the climatic  
52 condition dominantly explains the spatial variation of the atmospheric self-adjustment.

53 Eq. (15) performed excellently in reproducing the  $x$  values from CR with  $\Phi$  and  $ET_p/E_{pmax}$  (Figure 4d). The NSE,  
54 RMSE, Pearson  $r$ , and  $p$ -bias between the predicted  $\tilde{x}$  and the  $x$  from CR were 0.93, 0.03, 0.96, and 0.0%, respectively.

### 55 **3.3 Evaluation of the CR and the advanced models against the grid $ET_{wb}$**

56 By multiplying  $\tilde{x}$  to the mean annual ratio between  $ET_p$  and  $ET_{eq}$ , we determined  $\tilde{\alpha}_e$  across the Australian land  
57 surfaces. The resulting  $\tilde{\alpha}_e$  values ranged within  $1.13 \pm 0.114$ , and the median value was almost equal to Ma et al.'s (2021)  
58 global estimate (1.10). They were relatively high in the northwestern and the northern part, while being below the mean in the  
59 southern and the eastern parts (Figure 5a). On 19% of the surfaces,  $\tilde{\alpha}_e$  values were unity, and thus they might become below  
60 the theoretical limit unless bounded.

61 We again generated CR  $ET_a$  using the spatially varying  $\tilde{\alpha}_e$  values (Figure 5b). The mean CR  $ET_a$  for 1998-2014  
62 ranged in  $249 \pm 78.8 \text{ mm a}^{-1}$  and  $530 \pm 172.0 \text{ mm a}^{-1}$  under arid and semi-arid climates, while it decreased to  $805.2 \pm 209 \text{ mm}$   
63  $\text{a}^{-1}$  and  $932 \pm 239 \text{ mm a}^{-1}$  in semi-humid and humid regions, respectively. The flux observations were still acceptably  
64 regenerated with the less biases than in the case of  $\alpha_e = 1.15$  (Figure 6a). The  $\tilde{\alpha}_e$  based on the Budyko framework significantly  
65 reduced the biases introduced by the constant  $\alpha_e$  in (semi-)humid basins. Albeit some biases remained, the water-balance  $ET_{wb}$   
66 for 1998-2014 in the CAMELS basins were better reproduced by using the spatially varying  $\tilde{\alpha}_e$  (Figure 6b).

67 To confirm the improved performance of the combined CR-Budyko method across Australia, we resampled the new  
68 CR  $ET_a$  estimates to  $0.5^\circ \times 0.5^\circ$  and compared them with the grid  $ET_{wb}$  data. The  $ET_a$  products by GLEAM, FluxCom, and  
69 ERA5-Land were evaluated with the grid evaluation reference. As shown, the CR method with a constant  $\alpha_e = 1.15$  overrated  
70 the mean annual  $ET_a$  along the eastern and the northern coastlines (Figure 7b), underperforming the physical, the machine-  
71 learning, and the land surface models (Figure 8a). Although the smaller  $\alpha_e = 1.10$  made the CR method perform better, its  
72 predictability was still poorer than the three advanced models, and the residual variation was as large as in the case of  $\alpha_e =$   
73  $1.15$  (Figure 8b).

74 In contrast, when employing the  $\tilde{\alpha}_e$  conditioned by local climate conditions, the same CR formulation could alleviate  
75 the overestimation along the coastlines (Figure 7c). The Budyko-function-based  $\tilde{\alpha}_e$  led the CR  $ET_a$  estimates to neatly agree

76 with the grid  $ET_{wb}$ , and the residual variance was much smaller than in the case of  $\alpha_e = 1.10$  (Figure 8c). The CR method with  
77  $\tilde{\alpha}_e$  clearly outperformed the three advanced models in reproducing the grid  $ET_{wb}$  estimates (Figure 8d-f). Although the  
78 referenced grid  $ET_{wb}$  has some error sources associated with upscaling of P and Q, our comparative evaluation suggests that  
79 conditioning  $\alpha_e$  with local climate conditions could substantially reduce the uncertainty of CR  $ET_a$  estimates in ungauged areas.

## 80 **4 Discussion**

### 81 **4.1 Constraining the CR with the Budyko framework for ungauged areas**

82 The CR explains the dynamic equilibrium between the atmospheric  $ET_p$  and the underlying moisture conditions, while  
83 the Budyko framework describes the steady-state water balance with climatic controls (i.e., P and  $ET_w$ ). The analytical link  
84 between the CR and the Budyko equations, hence, implies that the atmospheric self-adjustment needs to be conditioned by the  
85 long-term climate conditions. Constraining the Turc-Mezentsev equation by the polynomial CR, Kim and Chun (2021) found  
86 that Q changes would be more sensitive to climatic changes than when they were not linked. In the opposite direction, the CR  
87 can be constrained by the Budyko equation to determine its essential parameter.

88 In Crago and Qualls (2018), the optimal  $\alpha_e$  for the linear CR of Crago et al. (2016) varied largely between 1.00 and  
89 1.43. This point-scale experiment has already suggested that a constant  $\alpha_e$  is unlikely suitable for definitive CRs to predict  $ET_a$   
90 in Australia. The ratio between the aerodynamic and the radiation components of  $ET_w$  is evidently affected by the heat  
91 entrainment from the top of the boundary layer (Baldocchi et al., 2016), the dissimilarity between heat and water vapor sources  
92 (Assouline et al., 2016), the large-scale synoptic changes (Guo et al., 2015), and the horizontal advection of dry air mass (Jury  
93 and Tanner, 1975). More recently, Han et al. (2021) proved the non-linear dependence of  $ET_w$  on  $ET_{eq}$ , and Yang and Roderick  
94 (2019) showed  $\alpha_e$  changing with  $R_n$  over ocean surfaces. Hence, the constant  $\alpha_e$  assumption underpinning the calibration-free  
95 CR is counterintuitive to the theoretical and empirical evidence. Although Ma et al. (2021) found some global applicability of  
96 the calibration-free CR, its performance remains unknown in most of the Australian surfaces and in many ungauged basins  
97 over the world.

98 Since  $ET_a$  plays a pivotal role in the terrestrial water and energy balances, the partitioning of  $R_n$  into the latent and  
99 the sensible heat fluxes cannot be independent of the partitioning of P into  $ET_a$  and Q. On a mean annual scale, P and  $ET_w$  are  
00 the major determinants of the P partitioning, and thus the parameter  $\alpha_e$  might not be independent of P. Given the large  
01 variability of P, assuming a fixed  $\alpha_e$  across a continental area may introduce considerable biases to CR  $ET_a$  estimates. Thus,  
02 discarding available P data may not be a good choice when predicting  $ET_a$  by the CR method in ungauged areas. It is  
03 noteworthy that  $\Phi$  dominantly explained the spatial variation of the mean annual x of the 71 CAMELS basins, and the  $\tilde{\alpha}_e$   
04 values conditioned by local climates were of a large spatial variation. This suggests that the CR with a constant  $\alpha_e$  may produce  
05 unreliable  $ET_a$  estimates in ungauged locations.

06           Nonetheless, the low performance with a constant  $\alpha_e$  does not indicate that the CR method underperforms the  
07 sophisticated  $ET_a$  models. The simple polynomial CR seemed to outperform the advanced the advanced physical, machine-  
08 learning, and land surface models, when its parameter was conditioned by local climates. The proposed CR-Budyko framework  
09 enabled to regionalize the optimal  $\alpha_e$  for the CR method from gauged basins to ungauged locations in an empirical manner. It  
10 should be highlighted that the CR with spatially varying  $\tilde{\alpha}_e$  produced the much smaller residual variance than the three  
11 advanced models.

## 12 **4.2 Remaining issues and caveats**

13           In seven Australian eddy-covariance flux towers, Crago et al. (2022) found that the optimal  $\alpha_e$  for the polynomial CR  
14 was 1.35 for predicting daily  $ET_a$  in the dimensionless form (i.e.,  $y = ET_a/ET_p$ ). However, it was increased to 1.42, 1.45, 1.47,  
15 and 1.50 to simulate the dimensional latent heat fluxes at daily, weekly, monthly, and annual timescales, respectively. This  
16 implies that the timescale would largely affect the optimal  $\alpha_e$  for the definitive CRs. Though the stationary Budyko equation  
17 can become a constraint at a mean-annual scale, how to capture the scale-dependence of  $\alpha_e$  is a remaining question.

18           Further questions also can arise as to how to quantify  $ET_p$  and  $E_{pmax}$ . For example, the  $\alpha_e$  values from  $ET_p$  with the  
19 Rome wind function rely upon an unrealistic assumption that the aerodynamic resistance on a vegetated surface is equivalent  
20 to that of an open-water surface. It is still unknown if this assumption is practically valid, because the Penman equation with  
21 the Rome wind function may result in unrealistically high  $ET_p$  even on a large wet area (McMahon et al., 2013). Given the  
22 importance of the aerodynamic resistance in modulating surface temperature (Chen et al., 2020), ignoring its variability may  
23 become a significant error source for the CR method at both annual and sub-annual timescales.

24           In addition, there are some caveats in our case study. We employed the meteorological data different from those used  
25 in Ma et al. (2021). The ERA5-Land dataset is a downscaled version of the ERA5 data (Hersbach et al., 2020) by which Ma  
26 et al. (2021) predicted  $ET_a$  globally. Ma et al. (2021) incorporated remotely sensed albedo and emissivity together with a  
27 correction factor when calculating  $R_n$ , whereas we used the sum of the ERA5-Land latent and sensible heat fluxes. Those input  
28 differences may lead to differences in CR  $ET_a$  estimates.

29           The gridded GRUN Q, too, has some uncertainty sources, though it is the ensemble of many runoff simulations from  
30 21 different atmospheric forcing inputs. In the machine-learning process by Ghiggi et al. (2021), some Q observations affected  
31 by human activities (e.g., dam regulation and return flows from groundwater abstraction) might not be excluded, potentially  
32 disrupting the empirical relationship between atmospheric forcing and natural flows. In addition, the uncertainty of SILO P  
33 might be non-negligible in areas with limited weather stations and in mountainous areas (Fu et al., 2022). Though we reduced  
34 the potential errors in the gridded P and Q datasets by temporal averaging, the grid-scale  $ET_{wb}$  estimates should be treated as  
35 plausible values rather than exact observations.

## 36 **5 Summary**

37 Via a case study in Australia, we showed that the polynomial CR by Szilagyi et al. (2017) is unlikely to perform well,  
38 when local climate conditions are neglected. The assumption of a constant Priestley-Taylor coefficient cannot reflect the long-  
39 term water balance; thereby, produced biased CR  $ET_a$  estimates. We resolved this problem by conditioning the CR with the  
40 traditional Budyko equation, and it allowed a reasonable determination of the essential parameter in ungauged locations. The  
41 following conclusions are worth emphasizing:

- 42 (1) The constant Priestley-Taylor coefficient transferred from fractional wet locations could make the CR method  
43 perform poorly in closing local water balance. The too simple approach could make the CR method underperform  
44 the widely used physical, machine-learning, and land surface models.
- 45 (2) The Budyko framework could become an additional constraint to determine the degree of  $ET_p$  adjustment at the  
46 mean annual scale. It allows upscaling of the Priestley-Taylor coefficients from gauged to ungauged locations.
- 47 (3) The Priestley-Taylor coefficients conditioned by local climates made the CR better close the basin-scale water  
48 balance. The varying Priestley-Taylor coefficients seemed to make the CR method outperform the advanced  $ET_a$   
49 models.

## 50 **Author contributions**

51 DK, MC, and JAC organized this study together. DK built the research framework, simulated  $ET_a$  with the CR method, and  
52 drafted the manuscript. JAC processed the modeled  $ET_a$  datasets and reviewed the draft, and MC actively participated in  
53 discussing the results.

## 54 **Competing interests**

55 The authors declare no competing interests.

## 56 **Code availability**

57 The Python scripts that implement the CR method are available upon request from the leading author (daeha.kim@jbnu.ac.kr).

## 58 **Acknowledgements**

59 This work was supported by Korea Environmental Industry & Technology Institute (KEITI) through Wetland Ecosystem  
60 Value Evaluation and Carbon Absorption Value Promotion Technology Development Project (2022003640001), funded by

61 Korea Ministry of Environment (MOE). We also acknowledge the financial support of the National Research Foundation of  
62 Korea (NRF) funded by the Korea government (MSIT) (NRF-2019R1A2B5B01070196).

### 63 **References**

- 64 Allen, R. G., Pereira, L. S., Raes, D., and Smith, M.: Crop evapotranspiration - Guidelines for computing crop water  
65 requirements - FAO Irrigation and drainage paper 56, Food and Agriculture Organization of the United Nations, Rome,  
66 1998.
- 67 Anayah, F. M., and Kaluarachchi, J. J.: Improving the complementary methods to estimate evapotranspiration under diverse  
68 climatic and physical conditions, *Hydrol. Earth Syst. Sci.*, 18, 2049–2064, <https://doi.org/10.5194/hess-18-2049-2014>, 2014.
- 69 Assouline, S., Li, D., Tyler, S., Tanny, J., Cohen, S., Bou-Zeid, E., Parlange, M., and Katul, G. G.: On the variability of the  
70 Priestley-Taylor coefficient over water bodies, *Water Resour. Res.*, 52, 150– 163, <https://doi.org/10.1002/2015wr017504>,  
71 2016.
- 72 Baldocchi, D. D.: How eddy covariance flux measurements have contributed to our understanding of Global Change Biology,  
73 *Glob. Change Biol.*, 26, 242– 260, <https://doi.org/10.1111/gcb.14807>, 2020.
- 74 Baldocchi, D., Knox, S., Dronova, I., Verfaillie, J., Oikawa, P., Sturtevant, C., Matthes, J. M., and Detto, M.: The impact of  
75 expanding flooded land area on the annual evaporation of rice, *Agric. Forest Meteorol.* 223, 181–193.  
76 <https://doi.org/10.1016/j.agrformet.2016.04.001>, 2016.
- 77 Balsamo, G., Albergel, C., Beljaars, A., Boussetta, S., Brun, E., Cloke, H., Dee, D., Dutra, E., Muñoz-Sabater, J.,  
78 Pappenberger, F., de Rosnay, P., Stockdale, T., and Vitart, F.: ERA-Interim/Land: a global land surface reanalysis data set,  
79 *Hydrol. Earth Syst. Sci.*, 19, 389–407. <https://doi.org/10.5194/hess-19-389-2015>, 2015.
- 80 Bouchet, R. J.: Evapotranspiration réelle et potentielle, signification climatique, in: General Assembly Berkeley, Int. Assoc.  
81 *Sci. Hydrol.*, Gentbrugge, Belgium, Publ. No. 62, 134–142, 1963.
- 82 Brutsaert, W., Cheng, L., and Zhang, L.: Spatial distribution of global landscape evaporation in the early twenty-first century  
83 by means of a generalized complementary approach, *J. Hydrometeorol.*, 21, 287–298, [https://doi.org/10.1175/JHM-D-19-](https://doi.org/10.1175/JHM-D-19-0208.1)  
84 [0208.1](https://doi.org/10.1175/JHM-D-19-0208.1), 2020.
- 85 Brutsaert, W., Li, W., Takahashi, A., Hiyama, T., Zhang, L., and Liu, W.: Nonlinear advection-aridity method for landscape  
86 evaporation and its application during the growing season in the southern Loess Plateau of the Yellow River basin, *Water*  
87 *Resour. Res.*, 53, 270–282. <https://doi.org/10.1002/2016WR019472>, 2017.
- 88 Brutsaert, W.: A generalized complementary principle with physical constraints for land-surface evaporation, *Water Resour.*  
89 *Res.*, 51, 8087–8093, <https://doi.org/10.1002/2015WR017720>, 2015.
- 90 Carmona, A. M., Poveda, G., Sivapalan, M., Vallejo-Bernal, S. M., and Bustamante, E.: A scaling approach to Budyko's  
91 framework and the complementary relationship of evaporation in humid environments: Case study of the Amazon River  
92 basin, *Hydrol. Earth Syst. Sci.*, 20, 589–603, <https://doi.org/10.5194/hess-20-589-2016>, 2016.

93 Chen, C., Li, D., Li, Y., Piao, S., Wang, X., Huang, M., Gentine, P., Nemani, R. R. and Myneni, R. B.: Biophysical impacts  
94 of Earth greening largely controlled by aerodynamic resistance, *Sci. Adv.*, 6, eabb1981,  
95 <https://doi.org/10.1126/sciadv.abb1981>, 2020.

96 Chen, X., and Buchberger, S. G.: Exploring the relationships between warm-season precipitation, potential evaporation, and  
97 “apparent” potential evaporation at site scale, *Hydrol. Earth Syst. Sci.* 22, 4535–4545. [https://doi.org/10.5194/hess-22-4535-](https://doi.org/10.5194/hess-22-4535-2018)  
98 2018, 2018.

99 Crago, R. D., and Qualls, R. J.: A graphical interpretation of the rescaled complementary relationship for evapotranspiration.  
00 *Water Resour. Res.*, 57, e2020WR028299. <https://doi.org/10.1029/2020WR028299>, 2021.

01 Crago, R. D., and Qualls, R. J.: Evaluation of the generalized and rescaled complementary evaporation relationships, *Water*  
02 *Resour. Res.*, 54, 8086–8102, <https://doi.org/10.1029/2018WR023401>, 2018.

03 Crago, R. D., and Qualls, R. J.: The value of intuitive concepts in evaporation research, *Water Resour. Res.*, 49, 6100–6104,  
04 <https://doi.org/10.1002/wrcr.20420>, 2013.

05 Crago, R. D., Qualls, R., and Szilagyi, J.: Complementary Relationship for evaporation performance at different spatial and  
06 temporal scales, *J. Hydrol.*, 608, 127575, <https://doi.org/10.1016/j.jhydrol.2022.127575>, 2022.

07 Crago, R., and Crowley, R.: Complementary relationships for near-instantaneous evaporation, *J. Hydrol.*, 300(1-4), 199–211,  
08 <https://doi.org/10.1016/j.jhydrol.2004.06.002>, 2005.

09 Crago, R., Szilagyi, J., Qualls, R., and Huntington, J.: Rescaling the complementary relationship for land surface evaporation,  
10 *Water Resour. Res.*, 52, 8461–8471, <https://doi.org/10.1002/2016WR019753>, 2016.

11 Fowler, K. J. A., Acharya, S. C., Addor, N., Chou, C., and Peel, M. C.: CAMELS-AUS: hydrometeorological time series and  
12 landscape attributes for 222 catchments in Australia, *Earth Syst. Sci. Data*, 13, 3847–3867, [https://doi.org/10.5194/essd-13-](https://doi.org/10.5194/essd-13-3847-2021)  
13 3847-2021, 2021.

14 Fu, B. P. (1981). On the calculation of evaporation from land surface. *Scientia Atmospherica Sinica*, 1, 23–31.

15 Fu, G., Barron, O., Charles, S. P., Donn, M. J., Van Niel, T. G., and Hodgson, G.: Uncertainty of gridded precipitation at local  
16 and continent scales: A direct comparison of rainfall from SILO and AWAP in Australia, *Asia-Pacific J. Atmos. Sci.*, in  
17 press, <https://doi.org/10.1007/s13143-022-00267-4>, 2022.

18 Ghiggi, G., Humphrey, V., Seneviratne, S. I., and Gudmundsson, L.: G-RUN ENSEMBLE: A multi-forcing observation-based  
19 global runoff reanalysis, *Water Resour. Res.*, 57, e2020WR028787, <https://doi.org/10.1029/2020WR028787>, 2021.

20 Glenn, E.P., Doody, T.M., Guerschman, J.P., Huete, A.R., King, E.A., McVicar, T.R., Van Dijk, A.I.J.M., Van Niel, T.G.,  
21 Yebra, M., and Zhang, Y.: Actual evapotranspiration estimation by ground and remote sensing methods: the Australian  
22 experience, *Hydrol. Process.*, 25, 4103–4116, <https://doi.org/10.1002/hyp.8391>, 2011

23 Guimberteau, M., Zhu, D., Maignan, F., Huang, Y., Yue, C., Dantec-Nédélec, S., Ottlé, C., Jornet-Puig, A., Bastos, A., Laurent,  
24 P., Goll, D., Bowring, S., Chang, J., Guenet, B., Tifafi, M., Peng, S., Krinner, G., Ducharne, A., Wang, F., Wang, T., Wang,  
25 X., Wang, Y., Yin, Z., Lauerwald, R., Joetzjer, E., Qiu, C., Kim, H., and Ciais, P.: ORCHIDEE-MICT (v8.4.1), a land

26 surface model for the high latitudes: model description and validation, *Geosci. Model Dev.*, 11, 121–163.  
27 <https://doi.org/10.5194/gmd-11-121-2018>, 2018.

28 Guo, X., Liu, H., and Yang, K.: On the application of the Priestley–Taylor relation on sub-daily time scales, *Boundary Layer*  
29 *Meteorol.*, 156, 489–499, <https://doi.org/10.1007/s10546-015-0031-y>, 2015.

30 Hagedorn, F., Gavazov, K., and Alexander, J. M.: Above- and belowground linkages shape responses of mountain vegetation  
31 to climate change, *Science*, 365, 1119–1123, <https://doi.org/10.1126/science.aax4737>, 2019. Han and Tian, 2018.

32 Han, S., and Tian, F.: Derivation of a sigmoid generalized complementary function for evaporation with physical constraints,  
33 *Water Resour. Res.*, 54, 5050– 5068, <https://doi.org/10.1029/2017WR021755>, 2018.

34 Han, S., Tian, F., Wang, W., and Wang, L.: Sigmoid generalized complementary equation for evaporation over wet surfaces:  
35 A nonlinear modification of the Priestley-Taylor equation, *Water Resour. Res.*, 57, e2020WR028737,  
36 <https://doi.org/10.1029/2020WR028737>, 2021.

37 Haverd, V., Smith, B., Nieradzic, L., Briggs, P. R., Woodgate, W., Trudinger, C. M., Canadell, J. G., and Cuntz, M.: A new  
38 version of the CABLE land surface model (Subversion revision r4601) incorporating land use and land cover change, woody  
39 vegetation demography, and a novel optimisation-based approach to plant coordination of photosynthesis, *Geosci. Model*  
40 *Dev.*, 11, 2995–3026, <https://doi.org/10.5194/gmd-11-2995-2018>, 2018.

41 Hersbach, H., Bell, B., Berrisford, P., Hirahara, S., Horányi, A., Muñoz-Sabater, J., Nicolas, J., Peubey, C., Radu, R., et al.:  
42 The ERA5 global reanalysis, *Q. J. R. Meteorol. Soc.* 146, 1999–2049. <http://doi.org/10.1002/qj.3803>, 2020.

43 Hobbins, M. T., Ramírez, J. A., and Brown, T. C.: Trends in pan evaporation and actual evapotranspiration across the  
44 conterminous U.S.: Paradoxical or complementary? *Geophys. Res. Lett.*, 31, L13503,  
45 <https://doi.org/10.1029/2004GL019846>, 2004.

46 Huntington, J. L., Szilagyi, J., Tyler, S. W., and Pohll, G. M.: Evaluating the complementary relationship for estimating  
47 evapotranspiration from arid shrublands, *Water Resour. Res.*, 47, W05533, <https://doi.org/10.1029/2010WR009874>, 2011.

48 Jasechko, S.: Plants turn on the tap, *Nature Clim. Change*, 8, 562–563, <https://doi.org/10.1038/s41558-018-0212-z>, 2018.

49 Jung, M., Koirala, S., Weber, U., Ichii, K., Gans, F., Camps-Valls, G., Papale, D., Schwalm, C., Tramontana, G., and  
50 Reichstein, M: The FLUXCOM ensemble of global land-atmosphere energy fluxes. *Sci. data*, 6, 74,  
51 <https://doi.org/10.1038/s41597-019-0076-8>, 2019.

52 Jury, W. and Tanner, C.: Advection modification of the Priestley and Taylor evapotranspiration formula, *Agron. J.*, 67, 840–  
53 842, <https://doi.org/10.2134/agronj1975.000219620>, 1975.

54 Kahler, D. M., and Brutsaert, W.: Complementary relationship between daily evaporation in the environment and pan  
55 evaporation, *Water Resour. Res.*, 42, W05413, <https://doi.org/10.1029/2005WR004541>, 2006.

56 Kim, D., and Chun, J. A.: Revisiting a two-parameter Budyko equation with the complementary evaporation principle for  
57 proper consideration of surface energy balance, *Water Resour. Res.*, 57, e2021WR030838,  
58 <https://doi.org/10.1029/2021WR030838>, 2021.

59 Kim, D., Ha, K.-J., and Yeo, J.-H.: New drought projections over East Asia using evapotranspiration deficits from the CMIP6  
60 warming scenarios, *Earths Future*, 9, e2020EF001697, <https://doi.org/10.1029/2020EF001697>, 2021.

61 Kim, D., Lee, W. -S., Kim, S. T., and Chun, J. A.: Historical drought assessment over the contiguous United States using the  
62 generalized complementary principle of evapotranspiration, *Water Resour. Res.*, 55, 6244–6267.  
63 <https://doi.org/10.1029/2019WR024991>, 2019.

64 Kyatengerwa, C., Kim, D., and Choi, M.: A national-scale drought assessment in Uganda based on evapotranspiration deficits  
65 from the Bouchet hypothesis, *J. Hydrol.*, 500, 124348, <https://doi.org/10.1016/j.jhydrol.2019.124348>, 2020.

66 Lhomme, J.-P., and Moussa, R.: Matching the Budyko functions with the complementary evaporation relationship:  
67 Consequences for the drying power of the air and the Priestley-Taylor coefficient, *Hydrol. Earth Syst. Sci.*, 20, 4857–4865,  
68 <https://doi.org/10.5194/hess-20-4857-2016>, 2016.

69 Ma, N., and Szilagyi, J.: The CR of evaporation: a calibration-free diagnostic and benchmarking tool for large-scale terrestrial  
70 evapotranspiration modeling. *Water Resour. Res.*, 55, 7246–7274, <https://doi.org/10.1029/2019WR024867>, 2019.

71 Ma, N., Szilagyi, J., and Zhang, Y.: Calibration-free complementary relationship estimates terrestrial evapotranspiration  
72 globally, *Water Resour. Res.*, 57, e2021WR029691, <https://doi.org/10.1029/2021WR029691>, 2021.

73 Ma, N., Szilagyi, J., Zhang, Y., and Liu, W.: Complementary-relationship-based modeling of terrestrial evapotranspiration  
74 across China during 1982–2012: validations and spatiotemporal analyses, *J. Geophys. Res. Atmos.*, 124, 4326–4351,  
75 <https://doi.org/10.1029/2018JD029850>, 2019.

76 Martens, B., Schumacher, D. L., Wouters, H., Muñoz-Sabater, J., Verhoest, N. E. C., and Miralles, D. G.: Evaluating the land-  
77 surface energy partitioning in ERA5, *Geosci. Model Dev.*, 13, 4159–4181, <https://doi.org/10.5194/gmd-13-4159-2020>,  
78 2020.

79 McMahon, T. A., Peel, M., Lowe, L., Srikanthan, R., and McVicar, T.: Estimating actual, potential, reference crop and pan  
80 evaporation using standard meteorological data: A pragmatic synthesis, *Hydrol. Earth Syst. Sci.*, 17, 1331–1363,  
81 <https://doi.org/10.5194/hess-17-1331-2013>, 2013.

82 Mekonnen, Z. A., Riley, W. J., Randerson, J. T., Grant, R. F., and Rogers, B. M.: Expansion of high-latitude deciduous forests  
83 driven by interactions between climate warming and fire, *Nature plants*, 5, 952–958, <https://doi.org/10.1038/s41477-019-0495-8>, 2019.

84

85 Mianabadi, A., Davary, K., Pourreza-Bilondi, M., and Coenders-Gerrits, A. M. J.: Budyko framework: Towards non-steady  
86 state condi- tions, *J. Hydrol.*, 588, 125089, <https://doi.org/10.1016/j.jhydrol.2020.125089>, 2020.

87 Miralles, D., G., Teuling, A., J. van Heerwaarden, C. C., and de Arellano, J. V.-G.: Mega-heatwave temperatures due to  
88 combined soil desiccation and atmospheric heat accumulation, *Nature Geosci.*, 7, 345–349,  
89 <https://doi.org/10.1038/ngeo2141>, 2014.

90 Mueller, B., and Seneviratne, S. I.: Hot days induced by precipitation deficits at the global scale, *P. Natl. Acad. Sci. USA*, 109,  
91 12398–12403, <https://doi.org/10.1073/pnas.1204330109>, 2012.

92 Muñoz-Sabater, J., Dutra, E., Agustí-Panareda, A., Albergel, C., Arduini, G., Balsamo, G., Boussetta, S., Choulga, M.,  
93 Harrigan, S., Hersbach, H., Martens, B., Miralles, D. G., Piles, M., Rodríguez-Fernández, N. J., Zsoter, E., Buontempo, C.,  
94 and Thépaut, J.-N.: ERA5-Land: a state-of-the-art global reanalysis dataset for land applications, *Earth Syst. Sci. Data*, 13,  
95 4349–4383, <https://doi.org/10.5194/essd-13-4349-2021>, 2021.

96 Novick, K. A., Biederman, J. A., Desai, A. R., Litvak, M. E., Moore, D. J. P., Scott, R. L., and Torn, M. S.: The AmeriFlux  
97 network: A coalition of the willing, *Agric. Forest Meteorol.*, 249, 444–456, <https://doi.org/10.1016/j.agrformet.2017.10.00>,  
98 2018. Pan et al. (2020)

99 Pan, S., Pan, N., Tian, H., Friedlingstein, P., Sitch, S., Shi, H., Arora, V. K., Haverd, V., Jain, A. K., Kato, E., Lienert, S.,  
00 Lombardozi, D., Nabel, J. E. M. S., Ottlé, C., Poulter, B., Zaehle, S., and Running, S. W.: Evaluation of global terrestrial  
01 evapotranspiration using state-of-the-art approaches in remote sensing, machine learning and land surface modeling, *Hydrol.*  
02 *Earth Syst. Sci.*, 24, 1485–1509, <https://doi.org/10.5194/hess-24-1485-2020>, 2020.

03 Pareek, A., Dhankher, O. P., and Foyer, C. H.: Mitigating the impact of climate change on plant productivity and ecosystem  
04 sustainability, *J. Exp. Bot.*, 71, 451–456, <https://doi.org/10.1093/jxb/erz518>, 2020.

05 Parlange, M. B., and Katul, G. G.: Estimation of the diurnal variation of potential evaporation from a wet bare soil surface, *J.*  
06 *Hydrol.*, 132, 71–89, [https://doi.org/10.1016/0022-1694\(92\)90173-s](https://doi.org/10.1016/0022-1694(92)90173-s), 1992. Qualls and Crago, 2020

07 Penman, H. L.: Natural evaporation from open water, bares soil, and grass, *Proc. R. Soc. Lond., Ser. A*, 193, 120–146.  
08 <https://doi.org/10.1098/rspa.1948.0037>, 1948.

09 Priestley, C. H., and Taylor, R. J.: On the assessment of surface heat flux and evaporation using large-scale parameters. *Mon.*  
10 *Weather Rev.*, 100, 81–92. [https://doi.org/10.1175/1520-0493\(1972\)100<0081:OTAOSH>2.3.CO;2](https://doi.org/10.1175/1520-0493(1972)100<0081:OTAOSH>2.3.CO;2), 1972.

11 Ramírez, J. A., Hobbins, M. T., and Brown, T. C.: Observational evidence of the complementary relationship in regional  
12 evaporation lends strong support for Bouchet's hypothesis, *Geophys. Res. Lett.*, 32, L15401,  
13 <https://doi.org/10.1029/2005GL023549>, 2005.

14 Rodriguez-Iturbe, I.: Ecohydrology: A hydrologic perspective of climate-soil-vegetation dynamics, *Water Resour. Res.*, 36,  
15 3–9, <https://doi.org/10.1029/1999WR900210>, 2000.

16 Schlosser, C. A., and Gao, X.: Assessing evapotranspiration estimates from the second global soil wetness project (GSWP-2)  
17 simulations, *J. Hydrometeorol.*, 11, 880–897, <https://doi.org/10.1175/2010jhm1203.1>, 2010.

18 Schumacher, D.L., Keune, J., van Heerwaarden, C.C., de Alrellano, J. V., Teuling, A. J., and Miralles, D. G.: Amplification  
19 of mega-heatwaves through heat torrents fuelled by upwind drought, *Nat. Geosci.*, 12, 712–717,  
20 <https://doi.org/10.1038/s41561-019-0431-6>, 2019.

21 Sun, Q., Miao, C., Duan, Q., Ashouri, H., Sorooshian, S., and Hsu, K.-L.: A review of global precipitation datasets: Data  
22 sources, estimation, and intercomparisons, *Rev. Geophys.*, 56, 79–107, <https://doi.org/10.1002/2017rg000574>, 2018.

23 Szilagyi, J., and Schepers, A.: Coupled heat and vapor transport: The thermostat effect of a freely evaporating land surface,  
24 *Geophys. Res. Lett.*, 41, 435–441, <https://doi.org/10.1002/2013gl058979>, 2014.

25 Szilagyi, J., Crago, R., and Qualls, R.: A calibration-free formulation of the complementary relationship of evaporation for  
26 continental-scale hydrology, *J. Geophys. Res. Atmos.*, 122, 264–278, <https://doi.org/10.1002/2016jd025611>, 2017.

27 Szilagyi, J.: On the thermodynamics foundations of the complementary relationship of evaporation, *J. Hydrol.*, 593, 125916,  
28 <http://doi.org/10.1016/j.jhydrol.2020.125916>, 2021.

29 Tramontana, G., Jung, M., Schwalm, C. R., Ichii, K., Camps-Valls, G., Ráduly, B., Reichstein, M., Arain, M. A., Cescatti, A.,  
30 Kiely, G., Merbold, L., Serrano-Ortiz, P., Sickert, S., Wolf, S., and Papale, D.: Predicting carbon dioxide and energy fluxes  
31 across global FLUXNET sites with regression algorithms, *Biogeosci.*, 13, 4291–4313, [https://doi.org/10.5194/bg-13-4291-](https://doi.org/10.5194/bg-13-4291-2016)  
32 2016, 2016.

33 Trenberth, K. E., Fasullo, J. T., and Kiehl, J.: Earth's global energy budget., *Bull. Am. Meteorol. Soc.*, 90, 311–324,  
34 <https://doi.org/10.1175/2008BAMS2634.1>, 2009.

35 Trenberth, K. E., Smith, L., Qian, T., Dai, A., and Fasullo, J.: Estimates of the global water Budget and its annual cycle using  
36 observational and model data, *J. Hydrometeorol.*, 8, 758–769, <https://doi.org/10.1175/JHM600.1>, 2007.

37 Wang, W., Xiao, W., Cao, C., Gao, Z., Hu, Z., Liu, S., Shen, S., Wang, L., Xiao, Q., Xu, J., Yang D., and Lee X.: Temporal  
38 and spatial variations in radiation and energy balance across a large freshwater lake in China, *J. Hydrol.*, 511, 811–824,  
39 <https://doi.org/10.1016/j.jhydrol.2014.02.012>, 2014.

40 Yang, H., Yang, D., Lei, Z., and Sun, F.: New analytical derivation of the mean annual water balance equation, *Water Resour.*  
41 *Res.*, 44, W03410, <https://doi.org/10.1029/2007WR006135>, 2008.

42 Yang, Y., and Roderick, M. L.: Radiation, surface temperature and evaporation over wet surfaces, *Q. J. R. Meteorol. Soc.*,  
43 145, 1118–1129, <https://doi.org/10.1002/qj.3481>, 2019.

44 Zhang, K., Zhu, G., Ma, J., Yang, Y., Shang, S., and Gu, C.: Parameter analysis and estimates for the MODIS  
45 evapotranspiration algorithm and multiscale verification, *Water Resour. Res.*, 55(3), 2211–2231,  
46 <https://doi.org/10.1029/2018wr023485>, 2019.

47 Zhang, L., and Brutsaert, W.: Blending the evaporation precipitation ratio with the complementary principle function for the  
48 prediction of evaporation, *Water Resou. Res.*, 57, e2021WR029729, <https://doi.org/10.1029/2021WR029729>, 2021

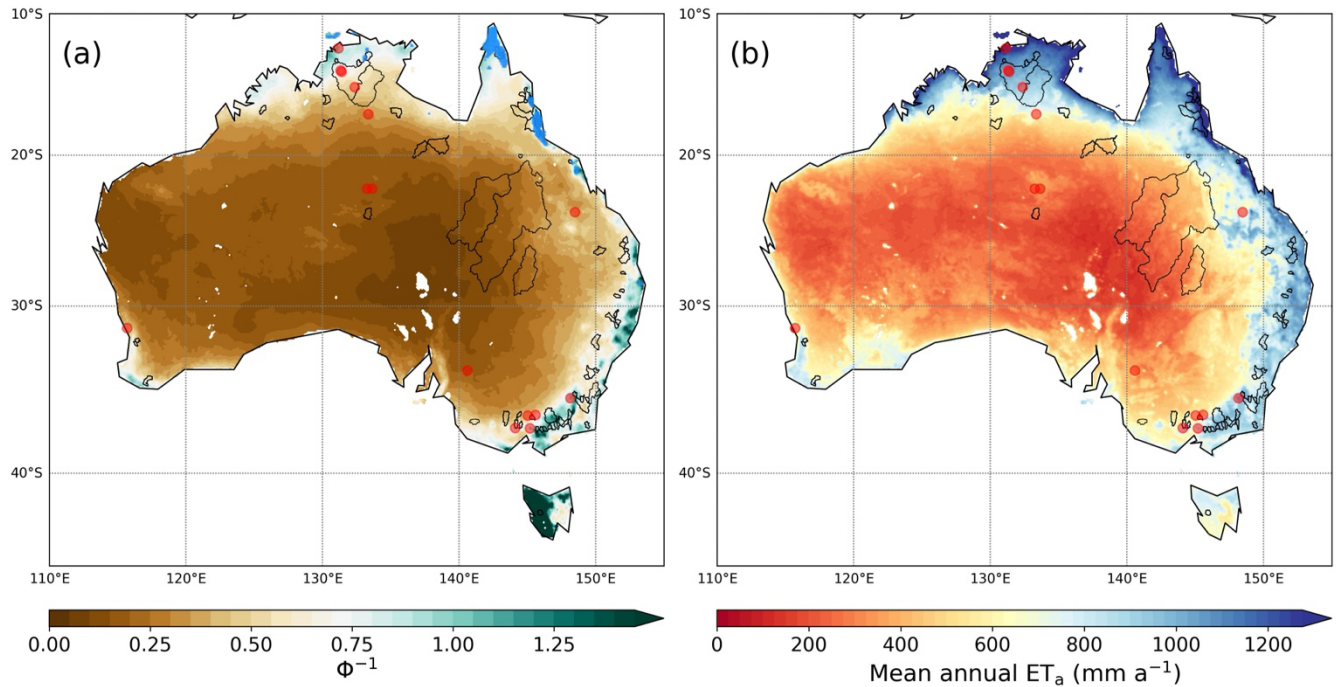
49 Zhang, Y., Peña-Arancibia, J. L., McVicar, T. R., Chiew, F. H., Vaze, J., Liu, C., Lu, X., Zheng, H., Wang, Y., and Liu, Y.  
50 Y.: Multi-decadal trends in global terrestrial evapotranspiration and its components, *Sci. Rep.*, 6, 19124,  
51 <https://doi.org/10.1038/srep19124>, 2016.

52 Zhou, S., Williams, A. P., Berg, A. M., Cook, B. I., Zhang, Y., Hagemann, S., Lorenz, R., Seneviratne, S. I., and Gentine, P.:  
53 Land–atmosphere feedbacks exacerbate concurrent soil drought and atmospheric aridity, *P. Natl. Acad. Sci. USA*, 116,  
54 18848–18853, <https://doi.org/10.1073/pnas.1904955116>, 2019.

55

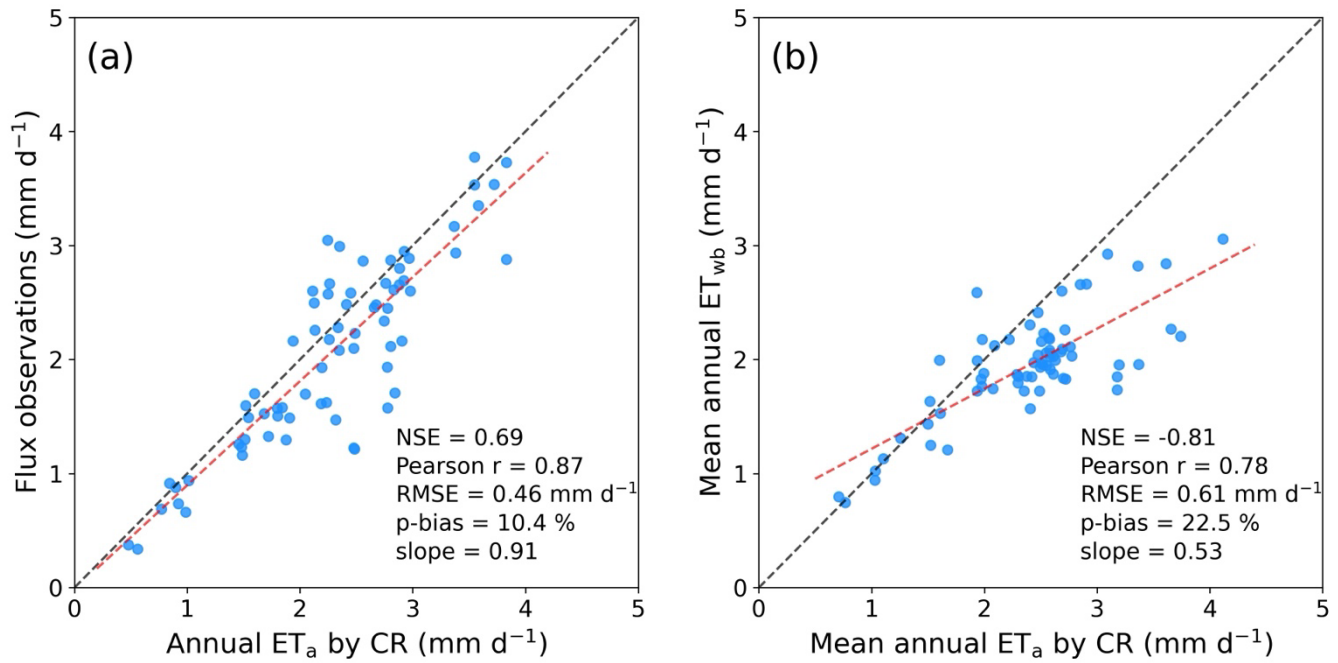
**Table 1. List of the chosen FLUXNET2015 sites**

Site ID	Lon. (°E)	Lat. (°S)	Data period	Site ID	Lon. (°E)	Lat. (°S)	Data period
AU-ASM	133.25	22.28	2010-2014	AU-Rig	145.58	36.65	2011-2014
AU-Cpr	140.59	34.00	2010-2014	AU-Stp	133.35	17.15	2008-2014
AU-DaP	131.32	14.06	2007-2013	AU-TTE	133.64	22.29	2012-2014
AU-DaS	131.39	14.16	2008-2014	AU-Tum	148.15	35.66	2001-2014
AU-Dry	132.37	15.26	2008-2014	AU-Wac	145.19	37.43	2005-2008
AU-Emr	148.47	23.86	2011-2013	AU-Whr	145.03	36.67	2011-2014
AU-Gin	115.71	31.38	2011-2014	AU-Wom	144.09	37.42	2010-2014
AU-How	131.15	12.49	2001-2014				



59

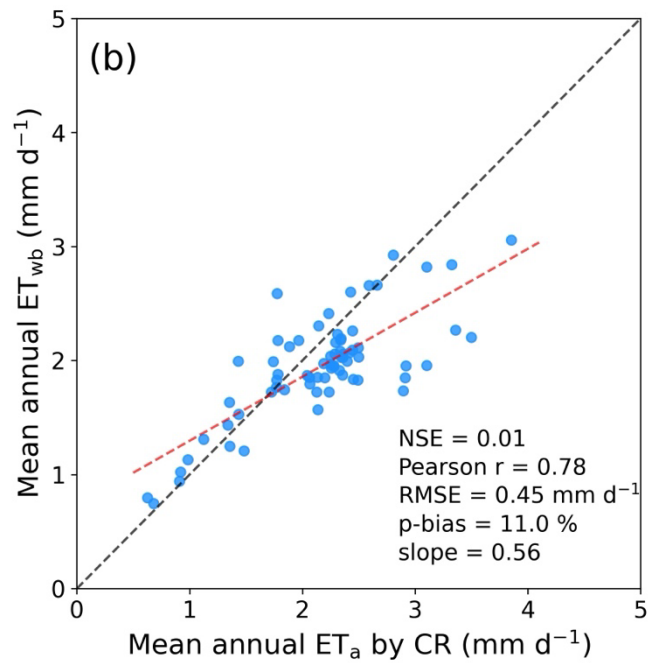
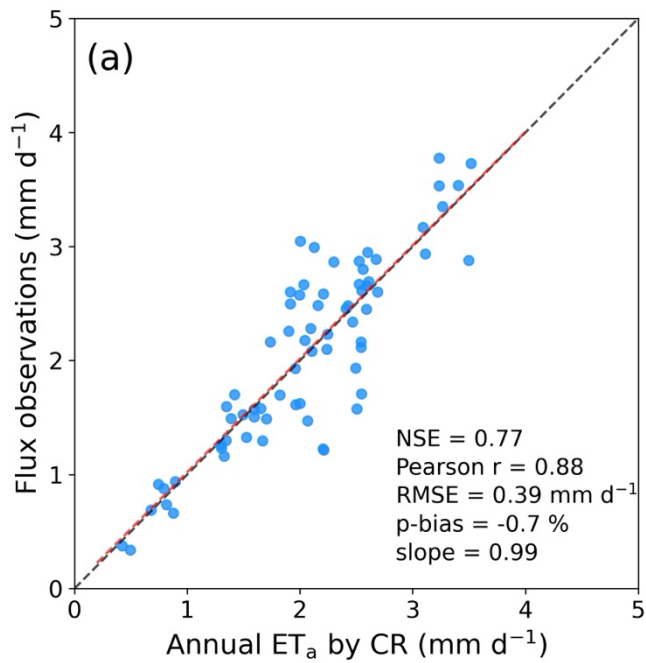
60 **Figure 1: Spatial distributions of (a) the reciprocals of aridity index and (b) the mean annual  $ET_a$  for 1998–2014 predicted by the**  
 61 **CR with  $\alpha_e = 1.15$ . The red circles and the gray polygons are the locations of 15 flux towers and the boundaries of 71 CAMELS**  
 62 **basins. The blue-colored points in (a) indicate the wet cells with  $RH > 90\%$  and  $T_{ws} > T_a + 2\text{ }^\circ\text{C}$ . CR  $ET_a$  was calculated at the grid**  
 63 **cells where the land fraction was larger than 50%.**



65

66 **Figure 2: The 1:1 comparison between the CR  $\text{ET}_a$  estimates with  $\alpha_c = 1.15$  and (a) the annual FLUXNET2015 observations and (b)**  
 67 **the mean annual  $\text{ET}_{\text{wb}}$  of the 71 CAMELS basins for 1998–2014.**

68

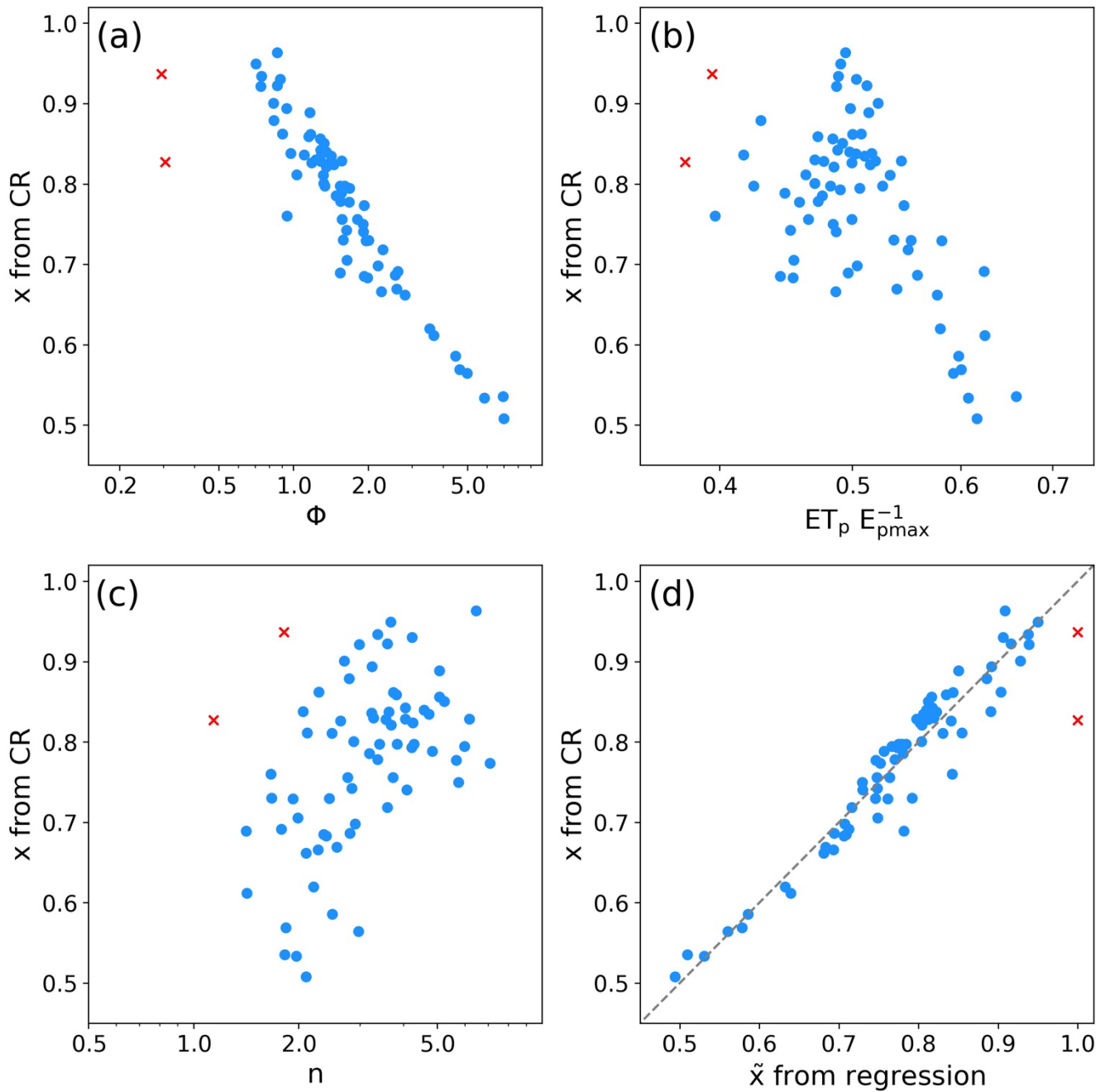


69

70

Figure 3: Same as Figure 2 except  $\alpha_e = 1.10$ .

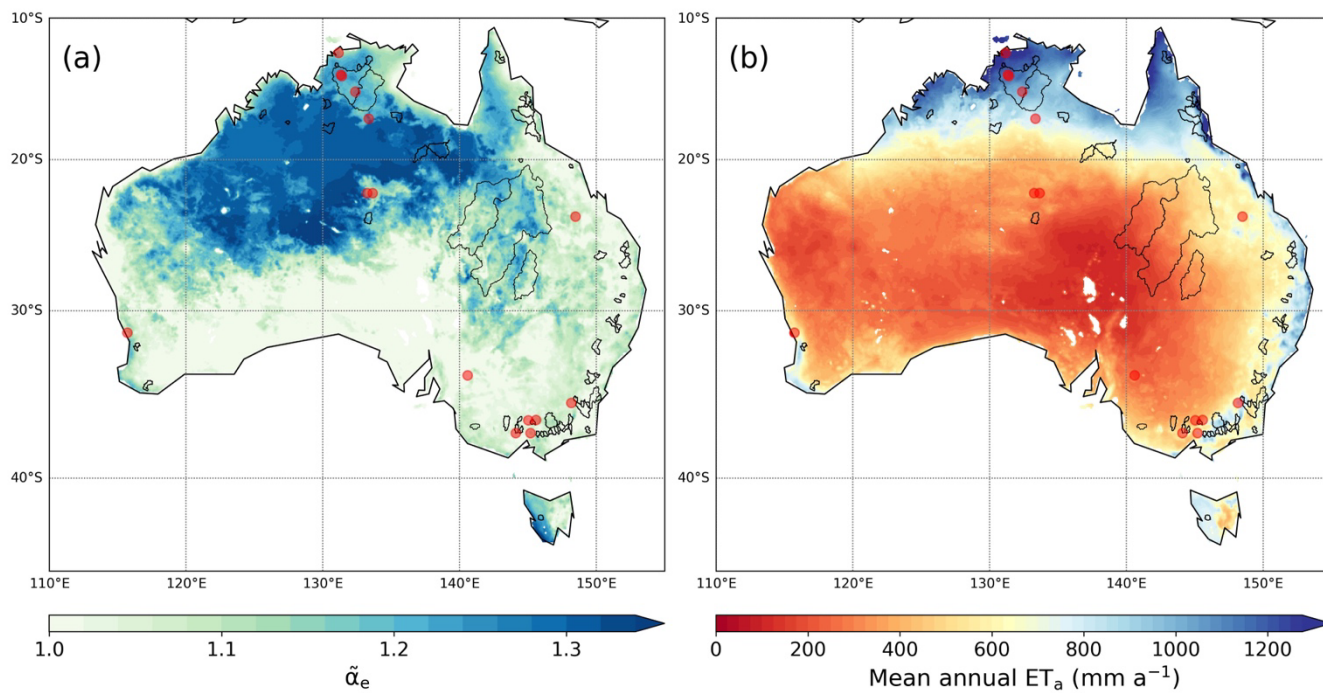
71



72  
73

74 **Figure 4: The scatter plots between the  $x$  estimated by CR with  $ET_{wb}$  for 1981-1997 and the corresponding (a)  $\Phi$ , (b)  $ET_p/E_{pmax}$ , and**  
 75 **(c)  $n$  values, and (d) the 1:1 plot between the  $x$  from CR and the  $\tilde{x}$  predicted by Eq. (15). The red  $x$  symbols are the outliers excluded**  
 76 **from the regression analysis.**

77



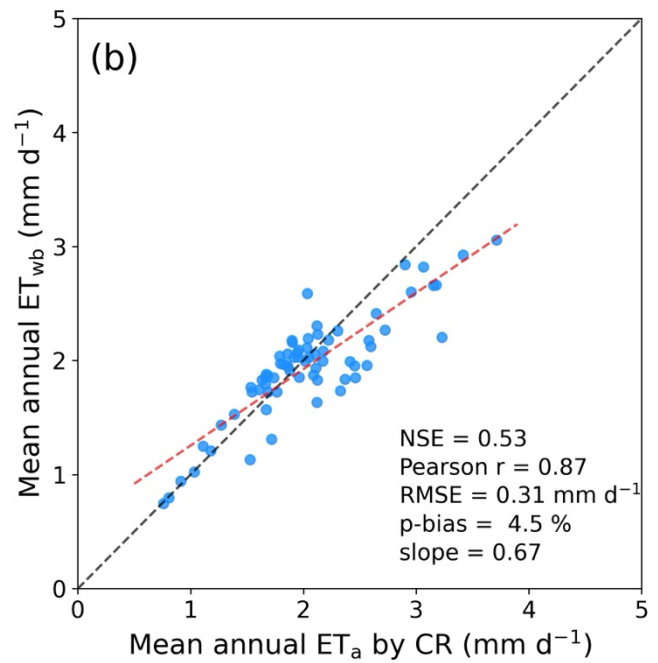
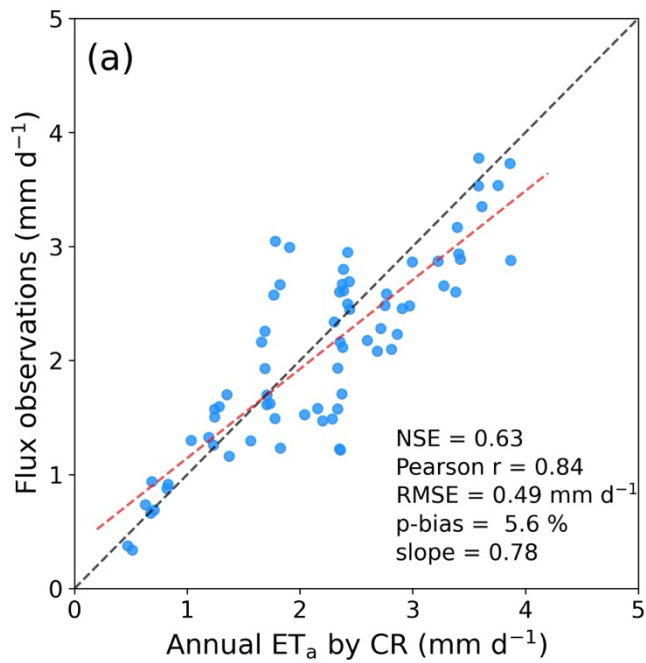
78

79

80

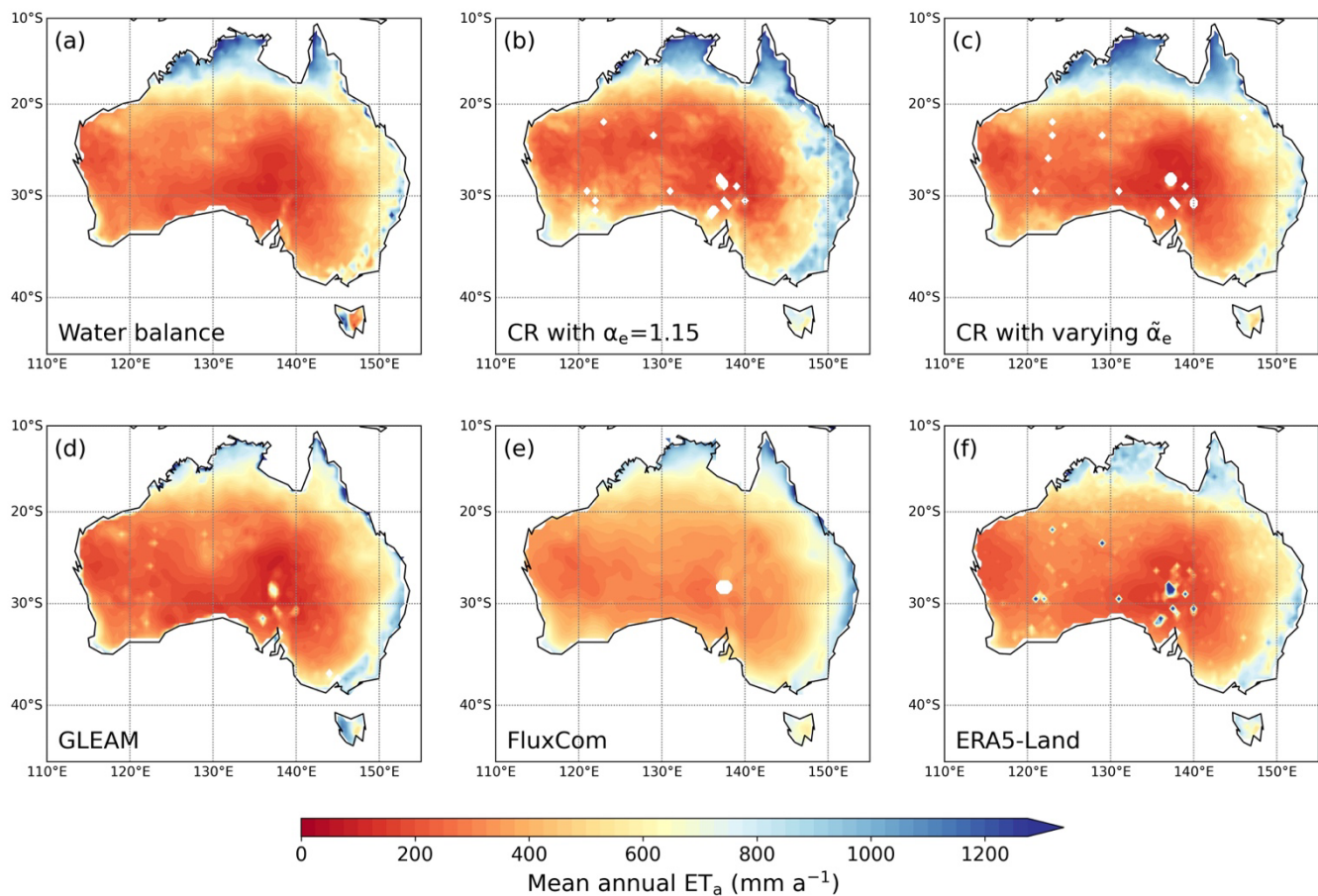
**Figure 5: Distributions of (a) the  $\tilde{\alpha}_e$  values from Eq. (15), and (b) the mean annual  $ET_a$  for 1998-2014 by the CR method and the  $\tilde{\alpha}_e$  values.**

81



82  
 83  
 84  
 85  
 86

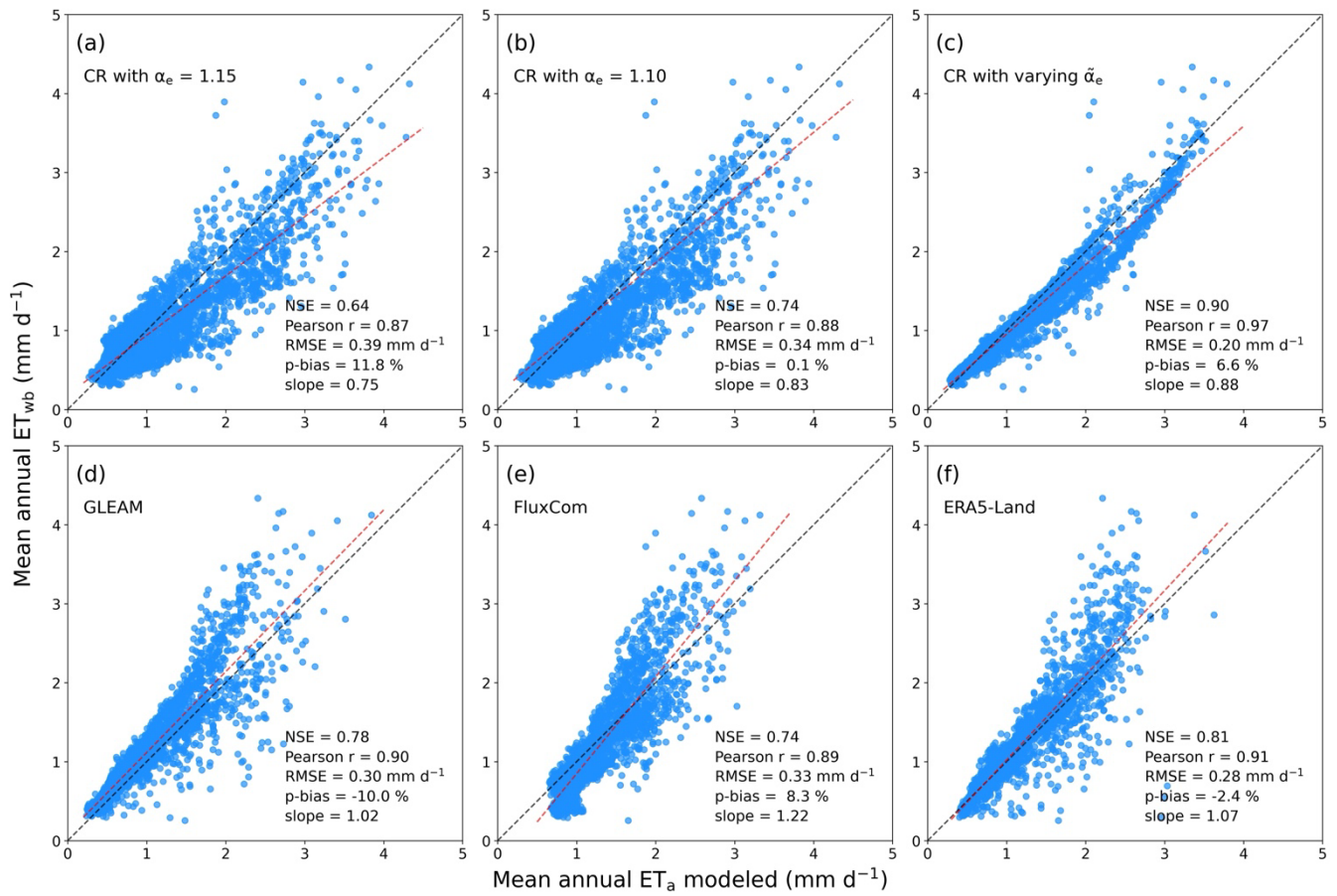
Figure 6: Same as Figure 2 except that the  $\tilde{\alpha}_e$  values from Eq. (15) were used for CR  $\text{ET}_a$ .



87

88 **Figure 7: Distributions of (a) the mean annual water-balance  $ET_{wb}$  for 1998–2014, and the predictions by (b) CR with  $\alpha_e = 1.15$ , (c)**  
 89 **CR with spatially varying  $\tilde{\alpha}_e$ , (d) GLEAM, (e) FluxCom, and (f) ERA5-Land.**

90



91

92 **Figure 8: Scatter plots between the mean annual  $ET_{wb}$  for 1998–2014 at  $0.5^\circ \times 0.5^\circ$  and the predictions by (a) CR with  $\alpha_e = 1.15$ , (b)**  
 93 **CR with  $\alpha_e = 1.10$ , (c) CR with spatially varying  $\tilde{\alpha}_e$ , (d) GLEAM, (e) FluxCom, and (f) ERA5-Land.**

94